JOURNAL OF TISSUE ENGINEERING AND REGENERATIVE MEDICINE
J Tissue Eng Regen Med (2011).
Published online in Wiley Online Library (wileyonlinelibrary.com) **DOI:** 10.1002/term.427

RESEARCH ARTICLE

Bone morphogenetic protein-2 in biodegradable gelatin and β-tricalcium phosphate sponges enhances the *in vivo* bone-forming capability of bone marrow mesenchymal stem cells

Mika Tadokoro[1], Asako Matsushima[1], Noriko Kotobuki[1], Motohiro Hirose[2], Yu Kimura[3], Yasuhiko Tabata[3], Koji Hattori[1] and Hajime Ohgushi[1]*

[1]*Health Research Institute, National Institute of Advanced Industrial Science and Technology (AIST), 3-11-46 Nakoji, Amagasaki, Hyogo 661-0974, Japan*
[2]*Human Technology Research Institute, National Institute of Advanced Industrial Science and Technology (AIST), 1-1-1 Higashi, Tsukuba, Ibaraki 305-8566, Japan*
[3]*Department of Biomaterials, Field of Tissue Engineering, Institute for Frontier Medical Sciences, Kyoto University, 53 Kawara-cho Shogoin, Sakyo-ku, Kyoto 606-8507, Japan*

Abstract

Bone marrow mesenchymal stem cells (MSCs) have been used for bone tissue engineering due to their osteogenic differentiation capability, but their application is controversial. To enhance their capability, we prepared biodegradable gelatin sponges incorporating β-tricalcium phosphate ceramics (GT sponge), which has been shown to possess excellent controlled drug-release properties. The GT sponge was used as a carrier for both rat MSCs and bone morphogenetic protein-2 (BMP-2) and osteogenic differentiation was assessed by subcutaneous implantation of four different kinds of implants, i.e. GT-alone, MSC–GT composites, BMP–GT composites and BMP–GT composites supplemented with MSCs (BMP–MSC–GT) in rats. Two weeks after implantation, histological sections showed new bone formation in the peripheral parts of the BMP–GT and in almost the total volume of the BMP–MSC–GT implants. After 4 weeks, histology as well as microCT analyses demonstrated extensive bone formation in BMP–MSC–GT implants. Gene expression and biochemical analyses of both alkaline phosphatase and bone-specific osteocalcin confirmed the histological findings. These results indicate that the combination of MSCs, GT and BMP synergistically enhances osteogenic capability and provides a rational basis for their clinical application in bone reconstruction. Copyright © 2011 John Wiley & Sons, Ltd.

Received 21 July 2010; Accepted 13 March 2011

Keywords gelatin; bone morphogenetic protein-2 (BMP-2); controlled drug release; mesenchymal stem cell; osteogenesis

1. Introduction

Bone defects have been clinically treated by implantation of various bone grafts or artificial bone graft substitutes. Autogenous bone is the gold standard for bone grafts because it has many advantages, including the absence of infections and biocompatibility, as well as osteoconductive and osteoinductive properties mediated via growth factors in the bone matrix. However, there are also many problems, such as quantitative limitations of the grafts and the inevitable invasion of normal tissues to harvest the bone graft. To avoid these problems, artificial bone substitutes, such as hydroxyapatite (HA) and β-tricalcium phosphate (β-TCP) ceramics, can be combined with collagen or other proteins and have

Correspondence to: Hajime Ohgushi, Health Research Institute, National Institute of Advanced Industrial Science and Technology (AIST), 3-11-46 Nakoji, Amagasaki, Hyogo 661-0974, Japan. E-mail: hajime-ohgushi@aist.go.jp

been used in clinical situations (LeGeros, 2008). Calcium phosphate ceramics are biocompatible, osteoconductive and bioactive, but it has been hard to conclusively show whether they have osteoinductive capability (Giannoudis *et al.*, 2005; Yoshikawa *et al.*, 2005).

It is now recognized that bone marrow is a major reservoir of mesenchymal stem cells (MSCs), which can differentiate not only into osteoblasts and chondrocytes, but also into other types of cells, such as hepatocytes, neural cells and stem cells that support haematopoiesis. MSCs have been regarded as the most reliable cell source for the purpose of bone tissue engineering after their combination with various scaffolds, including ceramics. We previously reported clinical application of autologous MSCs derived from patients' bone marrow for the treatment of bone diseases (Kawate *et al.*, 2006; Morishita *et al.*, 2006; Ohgushi *et al.*, 2004, 2005). However, in some cases, the osteogenic potential of the MSCs was not high enough for a good clinical outcome. If the potential could be increased by the addition of growth factors, promising results and an early start to rehabilitation could be achieved.

Growth factors such as bone morphogenetic proteins (BMPs), transforming growth factor-β (TGF-β) and basic fibroblast growth factor (bFGF) have been used to enhance bone regeneration. Among them, BMPs are reported to be useful in healing bone defects because of their osteoinductive properties. In particular, BMP-2 has been well characterized and is a very potent osteoinductive growth factor (Ikeuchi *et al.*, 2002; Reddi and Cunningham, 1993; Tabata, 2008, 2009; Zegzula *et al.*, 1997). However, the administration of BMP-2 in orthopaedic applications is restricted, due to its short biological half-life and localized actions (Ruhe *et al.*, 2006). To overcome these problems, incorporation of BMP-2 into biomaterials is necessary for its effective delivery at the *in vivo* implanted target site.

We previously developed biodegradable gelatin sponges incorporating β-TCP (GT) for the controlled release of BMP-2 (Takahashi *et al.*, 2005a, b). The controlled release of growth factors from gelatin results from the enzymatic degradation of gelatin, and the extent of gelatin crosslinking affects its degradation (Tabata *et al.*, 1999). Many studies have shown that GT sponge is an excellent carrier for various kinds of growth factors, but the efficacy of the sponge as a BMP-2 carrier, particularly for *in vivo* osteogenic potential of MSCs, is not clear. Here we show that the osteogenic potential of MSCs was accelerated by the high activity of BMP-2 incorporated into GT sponge, and therefore the combination of GT sponge, BMP-2 and MSCs could be used as an ideal approach for the purpose of bone tissue engineering.

2. Materials and methods

2.1. Preparation of mesenchymal stem cells

MSCs were derived from the femora of 7 week-old, male Fischer 344 rats, as previously described (Maniatopoulos *et al.*, 1988; Ohgushi *et al.*, 1996). The bone marrow was flushed out using 10 ml culture medium expelled from a syringe through a 21-gauge needle. The bone marrow was cultured in T-75 flasks containing 15 ml culture medium, consisting of minimum essential medium (MEM; Nacalai Tesque, Kyoto, Japan) with 15% fetal bovine serum (FBS; JRH Bioscience, KS, USA), 100 U/ml penicillin, 0.1 mg/ml streptomycin and 0.25 μg/ml amphotericin B (Nacalai Tesque). To remove non-adherent cells, the medium was changed after 2 days and subsequently renewed three times/week. Adherent cells were expanded as monolayer cultures in a humidified atmosphere of 5% CO_2 and 95% air at 37 °C. After 7 days of cultivation, the confluent cells were dissociated with 0.25% trypsin–EDTA and used for all experiments. To confirm the osteogenic capability of BMP-2 to differentiate MSCs into osteoblasts, MSCs were cultured with different amounts of BMP-2.

2.2. Preparation of gelatin-β-TCP sponges incorporating BMP-2

The manufacturing procedure of gelatin-β-TCP sponges used in this study was described previously (Takahashi *et al.*, 2005a, 2005b). In brief, an aqueous solution of gelatin and 50 wt% β-TCP granules (average diameter 2 μm; Taihei Chemical Industries, Nara, Japan) were mixed with a homogenizer. After addition of aqueous glutaraldehyde solution, the mixed solution was cast into a polypropylene dish and left at 4 °C for 12 h to allow gelatin cross-linking. Cross-linked gelatin sponges with β-TCP were then placed into aqueous glycine solution to block the residual aldehyde groups of glutaraldehyde. After washing with double-distilled water, the sponges were freeze-dried and cut into pieces 5 mm in diameter × 2 mm thick.

Commercially available gelatin sponge (Spongel®; Astellas Pharma, Tokyo, Japan) was used as a control for the GT sponges. The gelatin sponges were stamped out using a punch in a disk 5 0 mm in diameter × 2 mm thick.

BMP-2 was dissolved to make a concentration of 0.25 μg/μl in Milli-Q water. To incorporate BMP-2, 20 μl BMP-2 solution was impregnated into the gelatin–β-TCP sponges, which were freeze-dried. Gelatin sponges incorporating BMP-2 were prepared similarly as controls.

2.3. Implantation of gelatin–β-TCP sponges incorporating BMP-2

As shown in Table 1, we prepared eight experimental groups of implants as follows: gelatin–β-TCP sponge

Table 1. Number of implants per experimental group

Implants*				
GT alone	MSC-GT composites	BMP-GT composites	BMP-MSC-GT composites	Harvest time after implantation (weeks)
15	15	15	15	2
15	15	15	15	4
Implants*				
Sp alone	MSC-Sp composites	BMP-Sp composite	BMP-MSC-Sp composites	Harvest time after implantation (weeks)
15	15	15	15	2
15	15	15	15	4

*Total number of implants in each group was 15. Fifteen samples were used for μ-CT ($n = 5$), histological analysis ($n = 3$), biochemical analysis ($n = 4$) and gene expression ($n = 3$) after implantation.

alone (GT); GT with MSCs (MSC–GT); GT with BMP-2 (BMP–GT); GT with MSCs and BMP-2 (BMP–MSC–GT); gelatin sponge alone (Sp); Sp with MSCs (MSC–Sp); Sp with BMP-2 (BMP–Sp); Sp with MSCs and BMP-2 (BMP–MSC–Sp). The MSCs were suspended in the culture medium at a concentration of 1×10^7/ml. Twenty μl (2×10^5 cells/sample) of the cell suspensions were loaded into the sponges (for the groups MSC–GT and MSC–Sp) or the sponges combined with BMP-2 (for the groups BMP–MSC–GT and BMP–MSC–Sp) and were incubated at 37 °C for 1 h before implantation. The number of implants is summarized in Table 1. The samples were implanted subcutaneously into Fischer 344 rats. Four subcutaneous pockets were created on each side of the rat's back; therefore, one sample from each of the eight groups was implanted into a separate pockets. The total number of recipient rats per time period was 10; consequently, each group received 15 implants. The implants were harvested at 2 and 4 weeks after implantation and analysed histologically and biochemically.

2.4. MicroCT analysis

After implantation, five implants were harvested and fixed in buffered formalin for 1 day. The implants were scanned using micro-computed tomography (μCT; Hitachi Medical, Tokyo, Japan) for visualization of new bone. μCT was performed on fixed samples at 55 kV and 150 μA. The analytical conditions were: precision mode, ×10.5 magnification with an image intensifier field of 1.8 inches, total of 256 sagittal sections scanned. The intensity of newly formed bone was defined as the same level intensity of the osseous tissue (2165–2550 LUT). Total volume and the number of bone detections were measured using the software package TRI3D-BON (Ratoc System Engineering, Tokyo, Japan) according to the methods we previously reported (Nishikawa *et al.*, 2004).

Table 2. Quantitative real-time PCR primers

Alkaline phosphatase (ALP)
Forward, 5′-GAC AAG AAG CCC TTC ACA GC-3′
Reverse, 5′-ACT GGG CCT GGT AGT TGT TG-3′
Osteocalcin (OCN)
Forward, 5′-AAG CCC AGC GAC TCT GAG TC-3′
Reverse, 5′-GCT CCA AGT CCA TTG TTG AGG-3′
Glyceraldehyde-3-phosphate dehydrogenase (GAPDH)
Forward, 5′-AAC GAC CCC TTC ATT GAC CTC-3′
Reverse, 5′-CCT TGA CTG TGC CGT TGA ACT-3′

2.5. Histological analysis

Three implants of each group were fixed using 10% neutral buffered formalin, decalcified, dehydrated and embedded in paraffin for histological analysis. Sections were stained with haematoxylin and eosin (H&E).

2.6. Gene expression and biochemical analysis of implants

Two and 4 weeks after implantation, total RNA was extracted from the implants using TRIzol reagent (Invitrogen, CA, USA) according to the manufacturer's instructions. Then cDNA templates were synthesized using RevaTra Ace cDNA kit (Totobo, Osaka, Japan), following the manufacturer's instructions. Samples incubated in the absence of reverse transcriptase were used as controls. Gene expression levels of alkaline phosphatase (ALP) and osteocalcin were measured using a quantitative real-time PCR cycler (qPCR; iCycler iQ system, BioRad, CA, USA). The QuantiTect SYBER Green PCR (Qiagen) was used according to the manufacturer's instructions. Primer sequences are listed in Table 2. In all experiments, appropriate negative controls without template were subjected to the same procedure to detect DNA contamination or carry-over. The data were standardized to the gene expression level of the endogenous control,

glyceraldehyde-3-phosphate dehydrogenase (*GAPDH*). This allowed for differences in the amount of total RNA added to each reaction to be taken into account.

For biochemical analysis, the ALP activity and osteocalcin contents of the implants were measured at 2 and 4 weeks post-implantation. After washing with PBS, the implants were homogenized in 1 ml 0.2% Triton-X 100 solution and sonicated for 5 min. After centrifuging, the supernatant was assayed for ALP activity as described above. To measure osteocalcin in the implants, osteocalcin was extracted from the sediment of the Triton-X 100 extract by decalcification, using a 20% formic acid solution for <24 h at 4 °C. After desalting, using a prepacked Sephadex G-25 column (NAP-5 column; GE Healthcare UK, Buckinghamshire, UK), the eluted protein fraction was lyophilized and subjected to a Rat Osteocalcin EIA Kit (Biomedical Technologies, MA, USA) according to the manufacturer's instructions.

2.7. Statistics

For multiple comparisons, the groups were compared by non-parametric Kruskal–Wallis test. When significant variance was demonstrated, differences between individual groups were determined using the Mann–Whitney U-test with Bonferroni correction. In all analysis, the significance level was set at $p < 0.05$.

3. Results

3.1. MicroCT analysis

GT sponges implanted subcutaneously into the backs of rats were retrieved for μCT and histological analysis 2 and 4 weeks after implantation. Typical μCT images of sagittal sections of the implants are shown in Figure 1. The GT sponges had a low intensity before implantation. μCT images of some implant groups using GT sponges showed an increase in intensity at 2 weeks. Four weeks after implantation, the images of both the BMP–GT and BMP–MSC–GT implants showed high-intensity (white) areas. In the implants using gelatin sponge (Sp), a high-intensity area was only observed in the BMP–MSC–Sp group 2 weeks after implantation.

As described in our previous report (Nishikawa *et al.*, 2004), we could define the high-intensity areas as new bone formation. The average volumes of bone in the GT sponge implants were $0.0043 \pm 0.0010\ mm^3$ in GT, $0.0057 \pm 0.0503\ mm^3$ in MSC–GT, $0.16010 \pm 0.1142\ mm^3$ in BMP–GT, and $5.8690 \pm 1.5267\ mm^3$ in BMP–MSC–GT composites, respectively. The numbers of detections of bone were 0 in GT, 1 in MSC–GT, 4 in BMP–GT and 5 in BMP–MSC–GT composite, respectively (Figure 2A, C). The number of bone detections in the BMP–MSC–Sp group was only one out of five samples 2 weeks after implantation. After 4 weeks, we could not detect newly formed bone in any implants of the Sp, MSC–Sp, BMP–Sp or BMP–MSC–Sp groups. We confirmed that control samples (GT-alone) showed a background level of X-ray absorbance (Figure 2B). β-TCP granules (2 μm average diameter) incorporated sponge did not appear in 3D imaging because the μCT had a resolution of about 5 μm.

3.2. Histological analysis

Histological evaluation confirmed that the high-intensity areas seen in the μCT scan corresponded to areas of newly formed bone. Two weeks after implantation, histological sections showed new bone formation with osteoblasts and osteocytes in both BMP–GT and BMP–MSC–GT implants (Figure 3A), although new bone formation was only observed in the peripheral areas of the BMP–GT implants, while bone was seen throughout the BMP–MSC–GT implants (Figure 3B). Newly formed bone was also detected in the BMP–MSC–Sp implants but not in Sp-alone, BMP–Sp or MSC–Sp implants 2 weeks after implantation. After 4 weeks, more extensive bone formation was observed in the BMP–GT and BMP–MSC–GT implants (Figure 3A, B). The bone tissue in both BMP–GT and BMP–MSC–GT implants showed many osteocytes together with abundant extracellular bone matrix. Some areas of the BMP–MSC–GT implants also showed the existence of bone marrow-like tissue. As described above, none of the Sp implants were detected in the implanted areas and therefore could not be harvested at the 4-week time point.

3.3. Alkaline phosphatase and osteocalcin expression of implants

The gene expression profiles of alkaline phosphatase (ALP) and osteocalcin in the implants were analysed by qPCR (Figure 4). The expression levels of *ALP* mRNA in the BMP–MSC–GT group were higher than in the other GT groups after 2 weeks. After 4 weeks, the expression levels of *ALP* mRNA in the MSC–GT, BMP–GT and BMP–MSC–GT groups increased. The expression levels of *osteocalcin* mRNA in the BMP–MSC–GT group were also higher than those of the other GT groups.

Biochemical measurement of ALP activity was significantly higher in BMP–MSC–GT than in the other GT groups at 2 weeks, but after 4 weeks the ALP activity levels decreased (Figure 4B). However, both the BMP–GT and BMP–MSC–GT groups had high ALP activity levels compared with the GT-alone and MSC–GT groups. ALP activity in the Sp implants was as low as the GT-alone group (data not shown). High osteocalcin levels were detected in the BMP–MSC–GT group 2 weeks after implantation and this increased five-fold after 4 weeks. The BMP–GT group also showed a similar increase between 2 and 4 weeks. The highest content was seen in the BMP–MSC–GT 4 weeks after implantation. These findings correlated well with the histological sections,

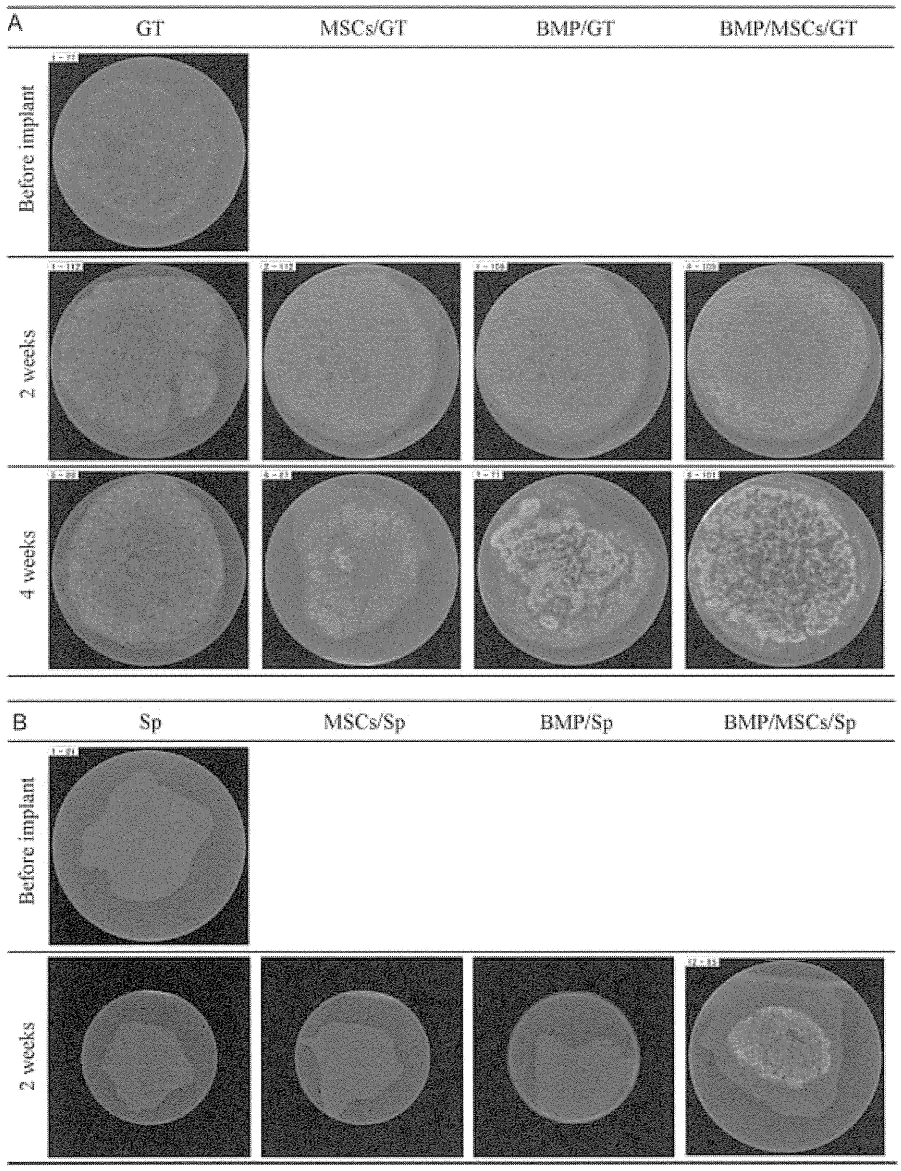

Figure 1. Typical micro-computed tomography (μCT) images of the implants using gelatin-β-TCP (GT) and gelatin (Sp) sponges. Images of various implants using GT (A) and Sp (B) materials after *in vivo* implantation. The MSC–GT, BMP–GT and BMP–MSC–GT implants show high-intensity areas (white) as compared to the image of the GT-alone implant 4 weeks after implantation

which showed abundant bone formation in the BMP–GT and BMP–MSC–GT groups and the *osteocalcin* gene expression profiles.

4. Discussion

Bone marrow-derived MSCs are a well-accepted source of osteogenic cells that can be used in bone tissue engineering. However, it is still a challenge to enhance the proliferation and differentiation of the *in vitro* expanded MSCs for bone tissue engineering, a problem that can be solved by approaches using growth factors (Betz *et al.*, 2008; Chan *et al.*, 2005). A number of factors have been shown to play a role in the osteogenic differentiation of MSCs (Kodama *et al.*, 2009; Maegawa *et al.*, 2007; Raiche and Puleo, 2004; Shimaoka *et al.*, 2004). In this study, we demonstrated that differentiation was greatly enhanced by BMP-2 *in vivo* using gelatin–β-TCP sponge incorporating BMP-2.

GT sponge could be fabricated to function as a release carrier of BMP-2. When BMP-2-incorporated GT sponges were implanted subcutaneously, the BMP-2 was retained in the sponges for at least 1 month and steadily released over that time. *In vivo* bone formation was observed in BMP-2-incorporated GT sponges 4 weeks after implantation in a subcutaneous site in rats (Takahashi *et al.*, 2005a). In this study, we aimed to demonstrate that early bone formation could be achieved by incorporating BMP-2 into GT sponges when combined with MSCs. As expected, we confirmed that new bone was observed in the BMP–MSC–GT and BMP–MSC–Sp groups 2 weeks after implantation. Furthermore, maturation of the new bone tissue was observed in the BMP–MSC–GT after

DOI: 10.1002/term

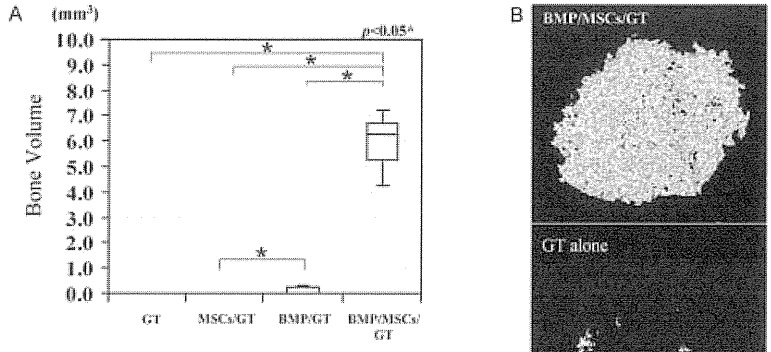

C

Implants	The average bone volume (mm³)	The Number of bone detections
GT alone	0.0043±0.0010	0/5
MSCs/GT composite	0.0057±0.0503	1/5
BMP/GT composites	0.1601±0.1142	4/5
BMP/MSCs/GT composites	5.8690±1.5267	5/5

Figure 2. Bone volume and 3D CT images of implants 4 weeks after subcutaneous implantation ($n = 5$). Bone volume (A) and 3D images (B) were calculated from μCT data. (C) Details of average bone volume and number of bone detections. $^{*}p < 0.05$

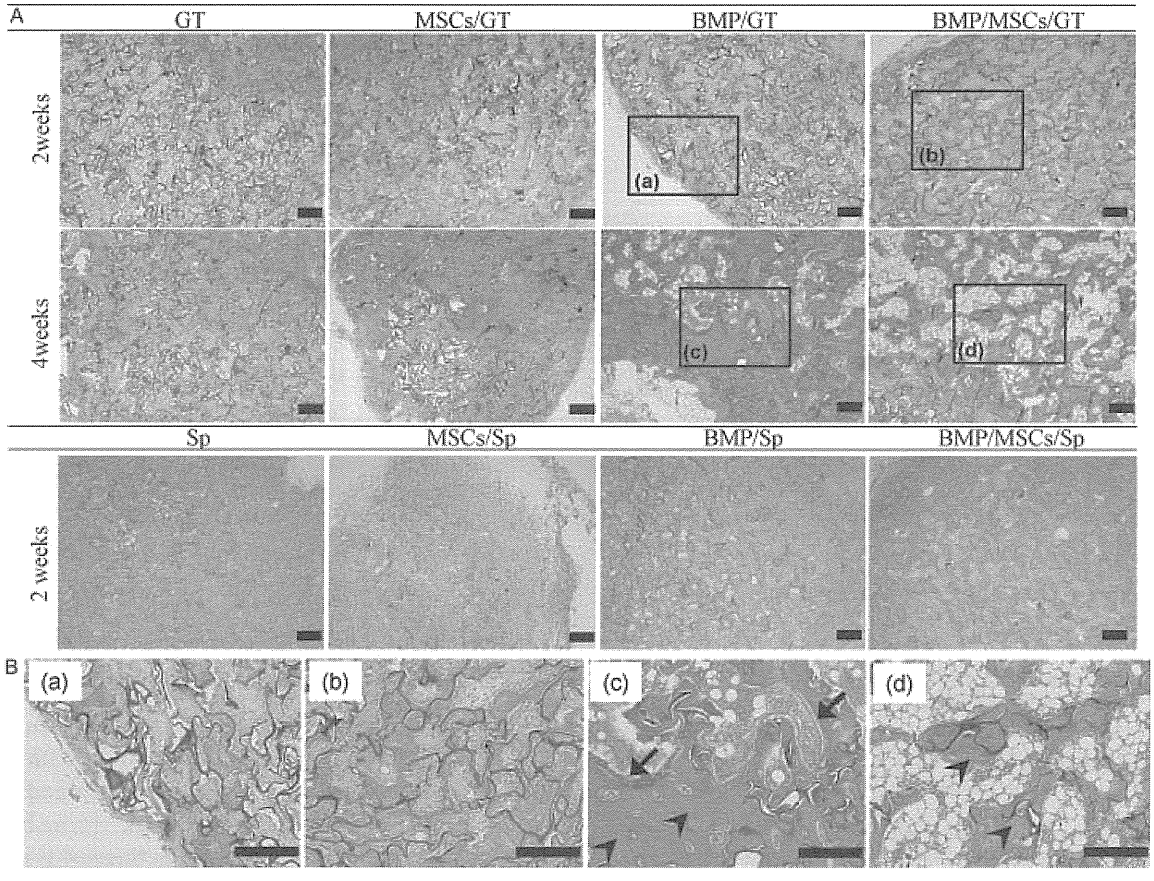

Figure 3. Histological findings of implants using gelatin-β-TCP (GT) and gelatin (Sp) sponges after implantation. (A) In implants using GT, new bone formation is observed in BMP–GT and BMP–MSC–GT implants 2 weeks after implantation. GT-alone and MSC–GT implants exhibit fibrous tissue invasion with no evidence of bone formation. Four weeks after implantation, massive bone formation is observed in the BMP–GT and BMP–MSC–GT implants. The GT-alone and MSC–GT implants exhibited fibrous tissue invasion but the bone formation was hard to detect. In Sp implants, new bone formation was observed in only BMP–MSC–Sp implants. The Sp alone, MSCs/Sp and BMS/Sp implants exhibited fibrous tissue invasion without bone formation. (B) High-magnification images of the rectangular areas of (a–c) and (e) in (A), respectively. Osteoblasts (arrows) and osteocytes (arrowheads) were observed within the newly formed bone. Scale bar = 200 μm

DOI: 10.1002/term

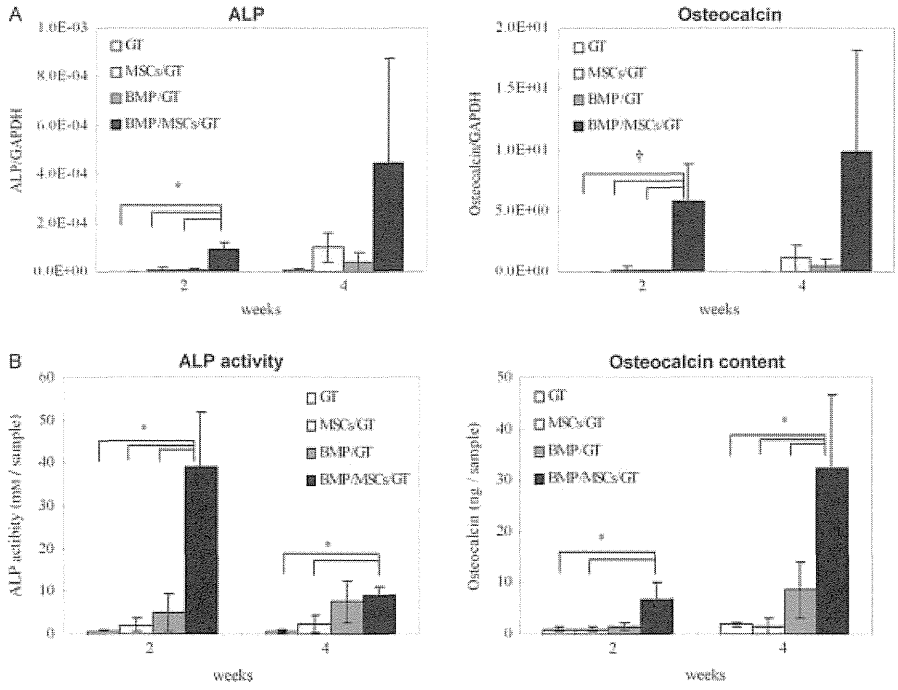

Figure 4. Gene expression and biochemical analysis of alkaline phosphatase (ALP) and osteocalcin in the implants. (A) The gene expression of ALP and osteocalcin were measured by quantitative real-time PCR 2 and 4 weeks after implantation. Values are shown as mean ± SD ($n = 3$). $^{*}p < 0.05$. $^{\dagger}p < 0.01$. (B) ALP activity and osteocalcin content of the implants were measured after 2 and 4 weeks. Implants are GT-alone, MSC–GT, BMP–GT and BMP–MSC–GT. Values are shown as mean ± SD ($n = 4$). $^{*}p < 0.05$

4 weeks. On the other hand, although new bone formation was observed in the BMP–GT group, which was free of MSCs, the volume of new bone was less than in the BMP–MSC–GT and the BMP–MSC–Sp groups. Biochemical analyses of the osteogenic differentiation at the levels of gene (Figure 4A) and protein expressions (Figure 4B) also demonstrated that the highest ALP and osteocalcin was in the BMP–MSC–GT group. These results indicate that the new bone-forming capability of BMP-2 incorporated into GT sponges could be enhanced by supplementation with MSCs.

We previously demonstrated that new bone formation was observed following subcutaneous implantation of MSCs combined with calcium phosphate ceramics, such as HA (Matsushima *et al.*, 2009; Ohgushi and Caplan, 1999; Okamoto *et al.*, 2006). However, the amount of new bone was limited 4 weeks after implantation and could not even be detected after 2 weeks. By adding BMP-2 into the HA ceramics, new bone formation increased, but in the composites of HA and BMP-2 without MSCs it was hard to identify the new bone (Shimaoka *et al.*, 2004). In contrast, the results from the present study clearly demonstrated the bone-forming capability of the BMP–GT implants, indicating the excellent ability of the GT to carry BMP-2. Furthermore, obvious bone formation was detected only 2 weeks after implantation in the BMP–MSC–GT group and extensive bone formation was observed in the composites after 4 weeks. With regard to β-TCP-containing sponge, β-TCP content did not change *in vivo* release behaviour of BMP-2 (Takahashi *et al.*, 2005b). However, in comparison with gelatin sponge incorporating other ceramics granules, such as HA, αTCP and alumina, gelatin-β-TCP sponges exhibited the highest ALP activity of MSCs among them (Takahashi *et al.* 2005b). These findings demonstrate the superior properties of GT sponge compared to HA ceramics.

One other disadvantage of the calcium phosphate ceramics is that absorption of the ceramics takes several months to years, and in the case of HA ceramics they are considered to be essentially non-absorbable. It is well known that the bone formation process followed by the absorptive capability of the implant, more specifically bone substitution, is an important factor for bone graft implantation in clinical situations. In this regard HA ceramics are not ideal materials, due to their poor absorption (Barrere *et al.*, 2006). However, too-early absorption hampers bone formation, as was seen in the BMP–MSC–Sp group as a result of the rapid absorptive properties of gelatin. Only one sample of the BMP–MSC–Sp group showed bone formation after 2 weeks, but none of the implants or bone tissue was detected after 4 weeks. We improved the absorption properties of the gelatin, which is known to have relatively rapid absorption properties compared with HA. Using the gelatin β-TCP sponge (GT), we successfully showed early bone formation with osteoblasts after 2 weeks and extensive bone tissue with many osteocytes in abundant bone matrix after 4 weeks.

5. Conclusion

Overall, the results presented here demonstrate the usefulness of the GT, BMP-2 and MSC composites as an

DOI: 10.1002/term

innovative osteoinductive bone graft substitute. Currently, gelatin, β-TCP, BMP-2 and MSCs have been used for various purposes in regenerative medicine. The ability of BMP-2 incorporated into GT sponges to form new bone could be enhanced by supplementation with MSCs. Moreover, the combination of GT sponge, BMP-2 and MSCs led to early bone formation. Due to the extensive *in vivo* bone formation together with reasonable GT absorption, the composites could be applied in tissue engineering aimed at bone tissue reconstruction.

Acknowledgements

This work was supported in part by the Project for Realization of Regenerative Medicine from the Ministry of Education, Culture, Sports, Science and Technology, Japan.

References

Barrere F, van Blitterswijk CA, de Groot K. 2006; Bone regeneration: molecular and cellular interactions with calcium phosphate ceramics. *Int J Nanomed* **1:** 317–332.

Betz VM, Betz OB, Harris MB, *et al.* 2008; Bone tissue engineering and repair by gene therapy. *Front Biosci* **13:** 833–841.

Chan J, O'Donoghue K, De la Fuente J, *et al.* 2005; Human fetal mesenchymal stem cells as vehicles for gene delivery. *Stem Cells* **23:** 93–102.

Giannoudis PV, Dinopoulos H, Tsiridis E. 2005; Bone substitutes: an update. *Injury* **36:** 20–27.

Ikeuchi M, Dohi Y, Horiuchi K, *et al.* 2002; Recombinant human bone morphogenetic protein-2 promotes osteogenesis within atelopeptide type I collagen solution by combination with rat cultured marrow cells. *J Biomed Mater Res* **60:** 61–69.

Kawate K, Yajima H, Ohgushi H, *et al.* 2006; Tissue-engineered approach for the treatment of steroid-induced osteonecrosis of the femoral head: transplantation of autologous mesenchymal stem cells cultured with β-tricalcium phosphate ceramics and free vascularized fibula. *Artif Organs* **30:** 960–962.

Kodama N, Nagata M, Tabata Y, *et al.* 2009; A local bone anabolic effect of rhFGF2-impregnated gelatin hydrogel by promoting cell proliferation and coordinating osteoblastic differentiation. *Bone* **44:** 699–707.

LeGeros RZ. 2008; Calcium phosphate-based osteoinductive materials. *Chem Rev* **108:** 4742–4753.

Maegawa N, Kawamura K, Hirose M, *et al.* 2007; Enhancement of osteoblastic differentiation of mesenchymal stromal cells cultured by selective combination of bone morphogenetic protein-2 (BMP-2) and fibroblast growth factor-2 (FGF-2). *J Tissue Eng Regen Med* **1:** 306–313.

Maniatopoulos C, Sodek J, Melcher AH. 1988; Bone formation *in vitro* by stromal cells obtained from bone marrow of young adult rats. *Cell Tissue Res* **254:** 317–330.

Matsushima A, Kotobuki N, Tadokoro M, *et al.* 2009; *In vivo* osteogenic capability of human mesenchymal cells cultured on hydroxyapatite and on β-tricalcium phosphate. *Artif Organs* **33:** 474–481.

Morishita T, Honoki K, Ohgushi H, *et al.* 2006; Tissue engineering approach to the treatment of bone tumors: three cases of cultured bone grafts derived from patients' mesenchymal stem cells. *Artif Organs* **30:** 115–118.

Nishikawa M, Myoui A, Ohgushi H, *et al.* 2004; Bone tissue engineering using novel interconnected porous hydroxyapatite ceramics combined with marrow mesenchymal cells: quantitative and three-dimensional image analysis. *Cell Transplant* **13:** 367–376.

Ohgushi H, Caplan AI. 1999; Stem cell technology and bioceramics: from cell to gene engineering. *J Biomed Mater Res* **48:** 913–927.

Ohgushi H, Dohi Y, Katuda T, *et al.* 1996; *In vitro* bone formation by rat marrow cell culture. *J Biomed Mater Res* **32:** 333–340.

Ohgushi H, Kitamura S, Kotobuki N, *et al.* 2004; Clinical application of marrow mesenchymal stem cells for hard tissue repair. *Yonsei Med J* **45:** 61–67.

Ohgushi H, Kotobuki N, Funaoka H, *et al.* 2005; Tissue engineered ceramic artificial joint – *ex vivo* osteogenic differentiation of patient mesenchymal cells on total ankle joints for treatment of osteoarthritis. *Biomaterials* **26:** 4654–4661.

Okamoto M, Dohi Y, Ohgushi H, *et al.* 2006; Influence of the porosity of hydroxyapatite ceramics on *in vitro* and *in vivo* bone formation by cultured rat bone marrow stromal cells. *J Mater Sci Mater Med* **17:** 327–336.

Raiche AT, Puleo DA. 2004; Cell responses to BMP-2 and IGF-I released with different time-dependent profiles. *J Biomed Mater Res A* **69A:** 342–350.

Reddi AH, Cunningham NS. 1993; Initiation and promotion of bone differentiation by bone morphogenetic proteins. *J Bone Miner Res* **8:** S499–502.

Ruhe PQ, Boerman OC, Russel FGM, *et al.* 2006; *In vivo* release of rhBMP-2 loaded porous calcium phosphate cement pretreated with albumin. *J Mater Sci Mater Med* **17:** 919–927.

Shimaoka H, Dohi Y, Ohgushi H, *et al.* 2004; Recombinant growth/differentiation factor-5 (GDF-5) stimulates osteogenic differentiation of marrow mesenchymal stem cells in porous hydroxyapatite ceramic. *J Biomed Mater Res A* **68A:** 168–176.

Tabata Y. 2008; Current status of regenerative medical therapy based on drug delivery technology. *Reprod Biomed Online* **16:** 70–80.

Tabata Y. 2009; Biomaterial technology for tissue engineering applications. *J Roy Soc Interface* **6:** S311–324.

Tabata Y, Nagano A, Ikada Y. 1999; Biodegradation of hydrogel carrier incorporating fibroblast growth factor. *Tissue Eng* **5:** 127–138.

Takahashi Y, Yamamoto M, Tabata Y. 2005a; Enhanced osteoinduction by controlled release of bone morphogenetic protein-2 from biodegradable sponge composed of gelatin and β-tricalcium phosphate. *Biomaterials* **26:** 4856–4865.

Takahashi Y, Yamamoto M, Tabata Y. 2005b; Osteogenic differentiation of mesenchymal stem cells in biodegradable sponges composed of gelatin and β-tricalcium phosphate. *Biomaterials* **26:** 3587–3596.

Yoshikawa H, Myoui A. 2005; Bone tissue engineering with porous hydroxyapatite ceramics. *J Artif Organs* **8:** 131–136.

Zegzula HD, Buck DC, Brekke J, *et al.* 1997; Bone formation with use of rhBMP-2 (recombinant human bone morphogenetic protein-2). *J Bone Joint Surg Am* **79A:** 1778–1790.

Ashdin Publishing
Bioceramics Development and Applications
Vol. 1 (2011), Article ID D110166, 4 pages
doi:10.4303/bda/D110166

Review Article

Forced Expression of Transcription Factors in Human Mesenchymal Cells to Promote Proliferation and Osteogenic Differentiation

Hiroe Ohnishi, Shunsuke Yuba, and Hajime Ohgushi

Health Research Institute, National Institute of Advanced Industrial Science and Technology (AIST), Amagasaki City, Hyogo 661-0974, Japan
Address correspondence to Hajime Ohgushi, hajime-ohgushi@aist.go.jp

Received 14 January 2011; Accepted 3 February 2011

Abstract Mesenchymal stromal cells (MSCs) derived from human bone marrow have capability to differentiate into cells of mesenchymal lineage [7]. Especially, the differentiation capability towards osteogenic cells is very well known. We have already used the patient's MSCs for the treatments of osteoarthritis [8], bone necrosis [2] and bone tumor cases [5]. In most cases, the MSCs were culture-expanded from patient's fresh bone marrow cells, and then combined with porous ceramics. The MSCs/ceramics composites were further cultured in a medium containing dexamethasone to promote osteogenic differentiation of the MSCs. In this culture condition, we could detect bone forming osteoblasts together with mineralized bone matrix on the ceramics [7]; therefore, we could fabricate cultured bone using patient's bone marrow and ceramics. However, the proliferation and differentiation capability of the MSCs are variable and many lose their capabilities after several passages. With the aim of conferring higher capability on human bone marrow MSCs, some of transcription factors could be introduced into the MSCs. This review paper demonstrates the importance of the transcription factors to promote the osteogenesis as well as proliferation capabilities of human MSCs.

Keywords mesenchymal stem cells (MSCs); osteogenesis; differentiation; transpription factor; cell culture; induced pluripotent stem cells (iPS cells)

1 Introduction

Embryonic stem (ES) cells are cultured cells derived from the inner cell mass of blastocysts. ES cells have pluripotency in that they can differentiate into cells of all lineages. Murine ES cells are commonly maintained on primary mouse embryonic fibroblast feeder cells in culture medium supplemented with bovine serum and leukaemia inhibitory factor (LIF). In the absence of LIF, murine ES cells differentiate spontaneously in serum containing culture medium [9]. In recent years, the mechanisms involved in maintaining the pluripotent state of human and mouse embryonic stem cells have been shown to differ. Whilst mouse embryonic stem cells are dependent upon the LIF, human ES cells are dependent on basic fibroblast growth factor (bFGF) to maintain self renewal, pluripotency and prevent differentiation [3].

In addition to these factors, Oct4, Nanog and Sox2 are considered to form transcriptional regulatory circuitry for pluripotency and self-renewal of ES cells [4] (Figure 1). These observations demonstrate a possibility that forced expression of these transcription factors could render bone marrow mesenchymal stromal cells (MSCs) better growth and plasticity properties, because the MSCs have limited proliferation and differentiation capabilities (Figure 2). In this paper, I focused on transcription factors especially Sox2 and Nanog aiming to elucidate the role of human MSCs in bone tissue engineering strategy.

2 Expression of transcription factors in human MSCs

We used the construct in which IRES sequence was placed between the gene of interest and the Venus gene, a variant of GFP, so that expression of the construct was easily detectable during the cell culture. Sox2-expressing cells

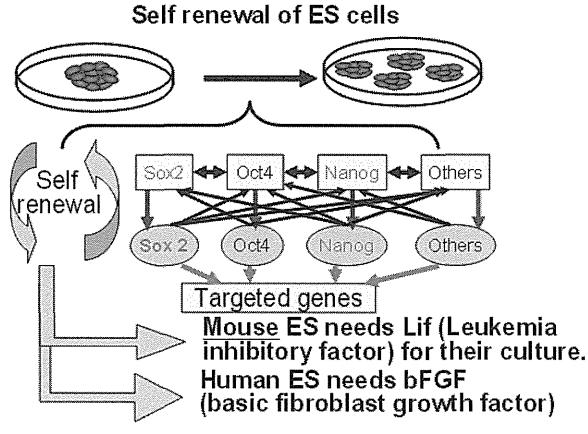

Figure 1: Transcription factors in ES cells.

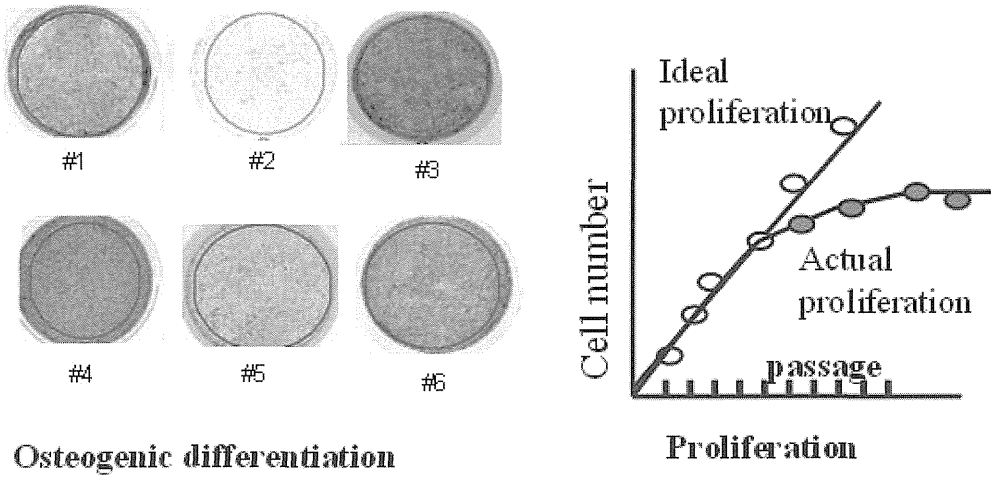

Figure 2: Proliferation and osteogenic differentiation capabilities among the patients.

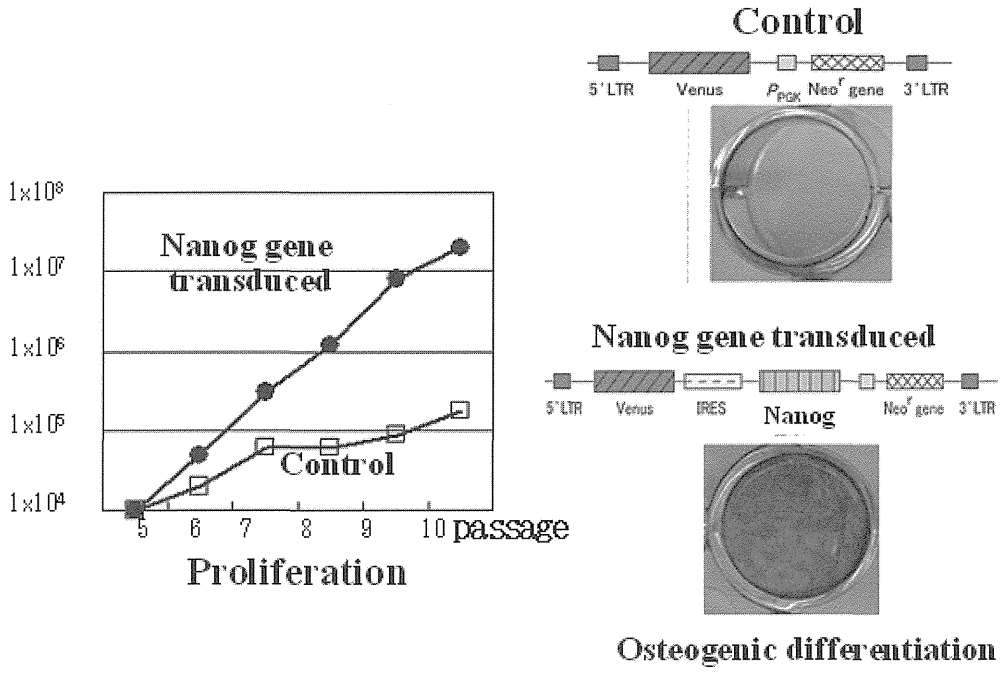

Figure 3: Nanog gene transduction into human mesenchymal cells.

showed distinct growth pattern in the presence of bFGF in culture media. In the presence of the bFGF protein in culture media, bone marrow MSCs show characteristic morphology changes, in which the cells become elongated in shape. In contrast, the Sox2-expressing MSCs responded to bFGF very differently, where the cells grew well as relatively round and small cells. The Sox2-expressing MSCs in the presence of bFGF had higher proliferation and osteogenic differentiation potential than control cells, in which only Venus was expressed [1].

We observed that Nanog-expressing MSCs were also relatively small and found that Nanog-expressing MSCs showed significantly higher proliferation potential than control cells (Figure 3). We failed to observe significant effects of addition of bFGF in culture media in the case of Nanog-expressing cells in terms of both cell growth ability and cell morphology change. We also found that Nanog-expressing cells showed higher differentiation abilities for osteoblasts than control cells both in terms of both ALP activity and calcium deposition assayed by Alizarin Red staining (Figure 3) [1].

Recently Yamanaka et al. reported that pluripotent stem cells can be directly generated from mouse [11] and human fibroblasts [10] by the introduction of several defined

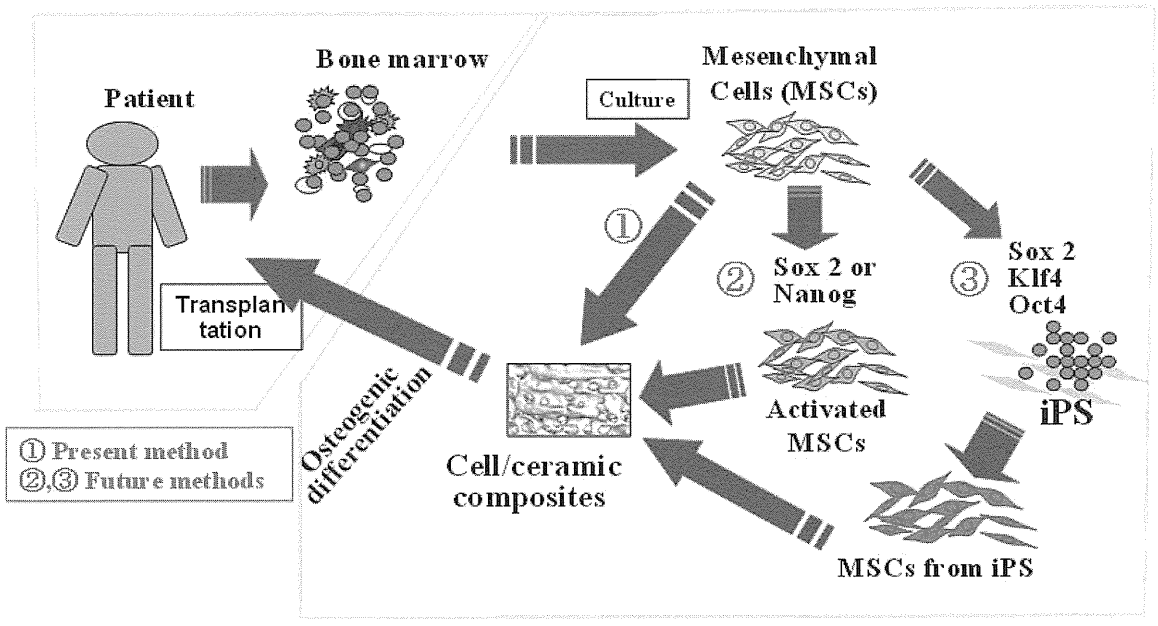

Figure 4: Current and future technologies for bone tissue engineering using MSCs.

genes, one of which was Sox2. Thomson et al. [12] also reported the generation of the induced pluripotent stem cells (iPS cells) by introduction of genes in which Nanog was included. These reports confirmed the importance of Sox2 and Nanog gene for the proliferation/differentiation capabilities of the stem cells. Though the single gene transduction is not sufficient to generate the iPS cells, the functional importance of Sox2 and Nanog for altering the cell status was clearly demonstrated.

3 Current and future technique for bone tissue engineering using MSCs

Our observations on the forced expression of Sox2 or Nanog in adult human MSCs are indeed consistent and succeeded to maintain the proliferation and osteogenic differentiation capabilities of otherwise senescent passaged cells by introducing single gene. We also experienced that these single gene expressing MSCs did not show teratoma formation, whereas the iPS cells have capability to show teratoma after their implantation. Based on our clinical experiences using patient's MSCs; serial passaged MSCs usually reduce their proliferation/differentiation capability (Figure 2). Therefore, our approach using single gene introduction could be an effective and realistic way of maintaining high quality of MSCs for regenerative medicine, especially for bone tissue regeneration. In addition, if we can solve the problem of teratoma formation after the iPS implantation, the iPS made from the patient cells could be available for bone tissue regeneration; especially in patients having severe bone diseases. Interestingly, we could generate the iPS cells from human MSCs and the iPS cells are indeed pluripotent stem cells because they could differentiate into cell types of all three germ layers [6]. These strategies using single and multiple gene transduction could be available in a near future as seen in Figure 4.

Acknowledgments The authors wish to acknowledge their staff at Research Institute for Cell Engineering, (RICE), National Institute of Advanced Industrial Science and Technology (AIST). They would like to acknowledge Dr. Go Masahiro and Miss Takanaka Chiemi for their works regarding Sox2/Nanog experiments and their colleagues at Nara Medical University.

References

[1] M. J. Go, C. Takenaka, and H. Ohgushi, *Forced expression of Sox2 or Nanog in human bone marrow derived mesenchymal stem cells maintains their expansion and differentiation capabilities*, Exp Cell Res, 314 (2008), 1147–1154.

[2] K. Kawate, H. Yajima, H. Ohgushi, N. Kotobuki, K. Sugimoto, T. Ohmura, et al., *Tissue-engineered approach for the treatment of steroid-induced osteonecrosis of the femoral head: transplantation of autologous mesenchymal stem cells cultured with beta-tricalcium phosphate ceramics and free vascularized fibula*, Artif Organs, 30 (2006), 960–962.

[3] M. E. Levenstein, T. E. Ludwig, R. H. Xu, R. A. Llanas, K. VanDenHeuvel-Kramer, D. Manning, et al., *Basic fibroblast growth factor support of human embryonic stem cell self-renewal*, Stem Cells, 24 (2006), 568–574.

[4] Y. H. Loh, Q. Wu, J. L. Chew, V. B. Vega, W. Zhang, X. Chen, et al., *The oct4 and Nanog transcription network regulates pluripotency in mouse embryonic stem cells*, Nat Genet, 38 (2006), 431–440.

[5] T. Morishita, K. Honoki, H. Ohgushi, N. Kotobuki, A. Matsushima, and Y. Takakura, *Tissue engineering approach to the treatment of bone tumors: three cases of cultured bone grafts derived from patients' mesenchymal stem cells*, Artif Organs, 30 (2006), 115–118.

[6] Y. Oda, Y. Yoshimura, H. Ohnishi, M. Tadokoro, Y. Katsube, M. Sasao, et al., *Induction of pluripotent stem cells from human third molar mesenchymal stromal cells*, J Biol Chem, 285 (2010), 29270–29278.

[7] H. Ohgushi and A. I. Caplan, *Stem cell technology and bioceramics: from cell to gene engineering*, J Biomed Mater Res, 48 (1999), 913–927.

[8] H. Ohgushi, N. Kotobuki, H. Funaoka, H. Machida, M. Hirose, Y. Tanaka, et al., *Tissue engineered ceramic artificial joint–ex vivo osteogenic differentiation of patient mesenchymal cells on total ankle joints for treatment of osteoarthritis*, Biomaterials, 26 (2005), 4654–4661.

[9] S. Pease, P. Braghetta, D. Gearing, D. Grail, and R. L. Williams, *Isolation of embryonic stem (ES) cells in media supplemented with recombinant leukemia inhibitory factor (LIF)*, Dev Biol, 141 (1990), 344–352.

[10] K. Takahashi, K. Tanabe, M. Ohnuki, M. Narita, T. Ichisaka, K. Tomoda, et al., *Induction of pluripotent stem cells from adult human fibroblasts by defined factors*, Cell, 131 (2007), 861–872.

[11] K. Takahashi and S. Yamanaka, *Induction of pluripotent stem cells from mouse embryonic and adult fibroblast cultures by defined factors*, Cell, 126 (2006), 663–676.

[12] J. Yu, M. A. Vodyanik, K. Smuga-Otto, J. Antosiewicz-Bourget, J. L. Frane, S. Tian, et al., *Induced pluripotent stem cell lines derived from human somatic cells*, Science, 318 (2007), 1917–1920.

Biochemical and Biophysical Research Communications 409 (2011) 1–6

Contents lists available at ScienceDirect

Biochemical and Biophysical Research Communications

journal homepage: www.elsevier.com/locate/ybbrc

Physical properties of mesenchymal stem cells are coordinated by the perinuclear actin cap

Takanori Kihara [a,*], Seyed Mohammad Ali Haghparast [a], Yuji Shimizu [a], Shunsuke Yuba [b], Jun Miyake [a]

[a] Department of Mechanical Science and Bioengineering, Graduate School of Engineering Science, Osaka University, 1-3 Machikaneyama, Toyonaka, Osaka 560-8531, Japan
[b] Health Research Institute, National Institute of Advanced Industrial Science and Technology (AIST), 3-11-46 Nakoji, Amagasaki, Hyogo 661-0974, Japan

ARTICLE INFO

Article history:
Received 4 April 2011
Available online 9 April 2011

Keywords:
Physical properties
Mesenchymal stem cells
Atomic force microscopy
Cell thickness and stiffness
Actin cytoskeleton
Perinuclear actin cap

ABSTRACT

Mesenchymal stem cells (MSCs) have been extensively investigated for their applications in regenerative medicine. Successful use of MSCs in cell-based therapies will rely on the ability to effectively identify their properties and functions with a relatively non-destructive methodology.

In this study, we measured the surface stiffness and thickness of rat MSCs with atomic force microscopy and clarified their relation at a single-cell level. The role of the perinuclear actin cap in regulating the thickness, stiffness, and proliferative activity of these cells was also determined by using several actin cytoskeleton-modifying reagents. This study has helped elucidate a possible link between the physical properties and the physiological function of the MSCs, and the corresponding regulatory role of the actin cytoskeleton.

1. Introduction

Mesenchymal stem cells (MSCs) are a heterogeneous population of stem/progenitor cells with the pluripotent capacity to differentiate into mesodermal and non-mesodermal cell lineages. They have generated a great deal of interest owing to their potential use in regenerative medicine and tissue engineering [1,2]. In order to maximize the potential of MSCs for biomedical applications, a more comprehensive characterization of MSCs is required. To achieve this goal, the development of a direct, relatively non-destructive method for measuring physical properties, which reflect the fate and physiological state of MSCs, is necessary. Population thickness (height) of adhered human MSCs may be related to various cell functions, such as proliferation activity and cell cycle [3,4]. However, a more comprehensive view of the physical properties of MSCs is required.

Mechanical properties such as cytoskeleton organization and elasticity, membrane tension, cell shape, and adhesion strength may play important roles in stem-cell fate and differentiation [5–7]. A change in mechanical properties, and in particular, in the stiffness (elasticity) of tissue cells, has been recognized as an indication of cancer [8]. Several techniques have been successfully employed to study cell mechanical properties, including micropipette aspiration, magnetic twisting cytometry, optical traps, and atomic force microscopy (AFM) [9–11]. In particular, AFM can be used to analyze live cells [12,13] and to investigate their mechanical properties in physiological conditions in a relatively non-destructive manner [14].

Surface mechanical properties of a cell are dominantly defined by the actin cytoskeleton [15–18]. Stress fibers are specific determinants of cell mechanics [19], and cortical actin promotes cortical rigidity [20,21]. Dominant types of actin cytoskeleton differ by cell types as well as position. Therefore, the key determinants for cell mechanics probably vary across different cell types, and it is necessary to determine the character of cell mechanics in each cell type.

Previously, we reported that the elastic modulus of human MSCs decreased dramatically by actin de-polymerization, whereas the cell thickness increased [22]. The elasticity and the thickness of an actin de-polymerized MSC and a bare nucleus were almost the same. Thus, regulatory factors of nuclear thickness and cell elasticity are possibly the same, and these may be related to the actin cytoskeleton. Recently, Khatau et al. reported that a perinuclear actin cap, which is an actin filament structure that forms a cap or dome above the apical surface of the nucleus, tightly regulates the nuclear shape of adherent fibroblasts [23]. In this study, we examined the regulatory effect of the perinuclear actin cap on thickness and stiffness of adherent rat MSCs by using several actin cytoskeleton-modifying drugs.

Abbreviations: MSC, mesenchymal stem cell; AFM, atomic force microscopy; FBS, fetal bovine serum; CLSM, confocal laser scanning microscopy.

* Corresponding author. Fax: +81 6 6850 6557.
E-mail address: takanori.kihara@gmail.com (T. Kihara).

0006-291X/$ - see front matter © 2011 Elsevier Inc. All rights reserved.
doi:10.1016/j.bbrc.2011.04.022

2. Materials and methods

2.1. Materials

The AFM probe (ATEC-CONT; spring constant: 0.02–0.75 N/m) was purchased from Nanosensors (Neuchatel, Switzerland). Cell culture media was purchased from Nacalai Tesque (Kyoto, Japan), and fetal bovine serum (FBS) was purchased from JRH Biosciences (Lenexa, KS). Antibiotics were purchased from Sigma–Aldrich (St. Louis, MO). Fisher 344 male rats were purchased from Japan SLC (Shizuoka, Japan). ATP bioluminescence assay kit was purchased from Toyo Ink (Tokyo, Japan). Other reagents were purchased from Sigma–Aldrich, Wako Pure Chemical Industries Ltd. (Osaka, Japan), or Invitrogen (Carlsbad, CA).

2.2. Preparation and culture of rat MSCs

Rat MSCs were isolated and primarily cultured as described previously [24]. In brief, bone marrow cells were obtained from the femoral shafts of 7-week-old male Fisher 344 rats. The cells were obtained from at least 2 rats and mixed. The culture medium was Eagle's minimal essential medium (with Earle's Salt and L-glutamine) containing 15% FBS and antibiotics (100 U/mL penicillin G, 100 μg/mL streptomycin sulfate, and 0.25 μg/mL amphotericin B). The medium was renewed twice a week, and cells at passages 2–6 were used in this study.

Y-27632 (10 μM), blebbistatin (5 μM), cell permeable C3 transferase (20 ng/mL), calyculin A (0.15 nM), and wiskostatin (1 μM) were used to analyze inhibition or acceleration of the actin cytoskeleton. Cells were cultured in the medium containing these reagents for 2 days and then manipulated by AFM.

2.3. AFM measurements

Rat MSCs cultured on 35-mm culture dishes in the medium were manipulated by AFM (Nanowizard I; JPK Instruments AG, Berlin, Germany) at room temperature. The probe was indented into the cells up to 50 nN at 10 μm/s. The Young's modulus of the cell was calculated according to the Hertz model [25]. Although the Hertz model is accommodated in an elastic body, various kinds of cellular stiffness have been evaluated by this model as Young's modules [26]. The force–distance curve at the region up to 400 nm of cell surface indentation was fitted to the model (Fig. 1A). Although the ATEC-CONT is a tetrahedral probe, the edge of the probe is conoidal. Thus, the following equation was used in the model of indentation:

$$F = \frac{E}{(1-\nu^2)}\frac{2\tan\alpha}{\pi}I^2$$

where F = force, I = depth of indentation, α = semi-opening angle of the cone (5°), ν = Poisson's ratio (0.5), and E = Young's modulus.

Cell thickness was derived from the length, from the cell contact point to the substrate (Fig. 1A). All experiments were performed in more than 10 cells, and each cell was examined at 9 different points within a size-defined grid on the nuclear region of the membrane. In this study, we assumed that the distribution of Young's moduli and the thickness of cells were in accordance with the

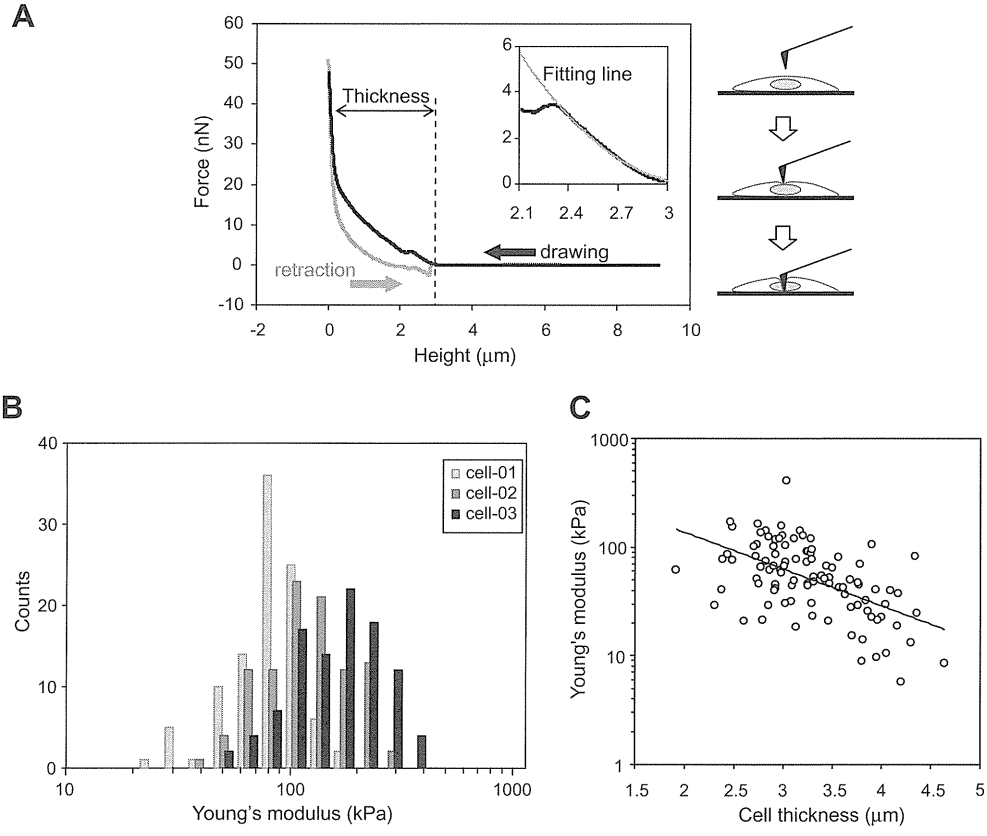

Fig. 1. Measurement of the cell stiffness and cell thickness of MSCs. (A) Details of the method of measuring cell stiffness and thickness by AFM. Typical force–distance curves obtained from the indentation of and pulling up from the surface of rat MSCs are shown at the left, and the schema for the AFM manipulation is shown at the right. Cell thickness is represented as the distance between the contact point of cell surface and substrate. Stiffness is calculated from the force curve at the region of indentation (up to 400 nm) by fitting it to the Hertz model (inset). (B) Distribution of Young's modulus of the same MSCs. Young's modulus of each cell (total of 3 cells) was measured 100 times repeatedly. The distribution pattern of Young's modulus of rat MSCs shows a log-normal pattern. (C) Relationship between the median value of Young's modulus and cell thickness in rat MSCs. Each data point is for one cell (total of 100 cells). The line shows approximated curve for the points (R = 0.35, P = 0.0004).

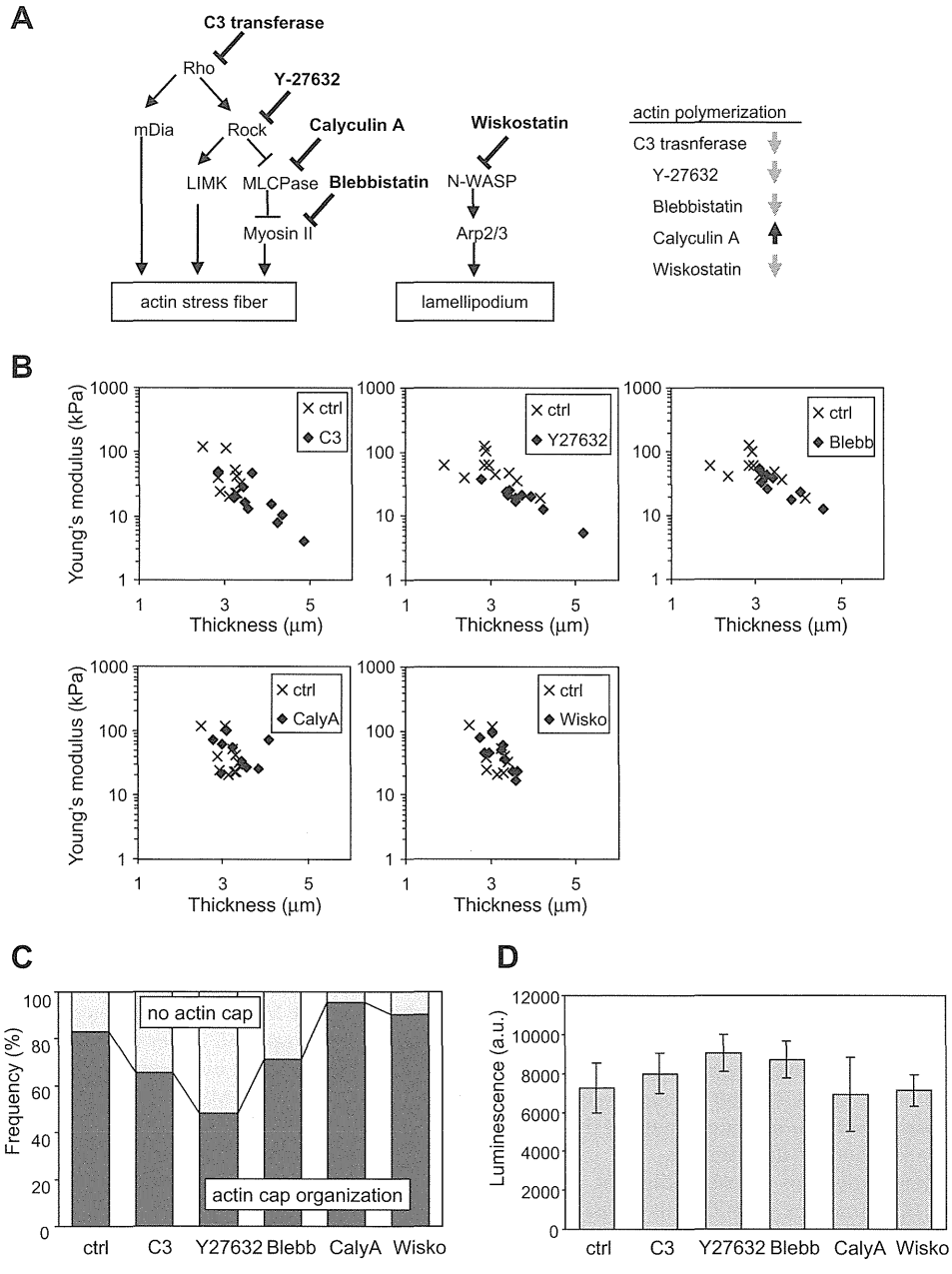

Fig. 2. Role of the actin cytoskeleton in regulating the cell properties of rat MSCs. (A) Schematics of effects of the used reagents on the actin cytoskeleton. C3 transferase, Y-27632, and blebbistatin inhibit actin polymerization and stress fiber formation. In contrast, calyculin A inhibits myosin light chain phosphatase and leads to actin polymerization, resulting in stress fiber and cortical actin formation. Wiskostatin inhibits lamellipodium formation. (B) Influence of the agents on Young's modulus and thickness of rat MSCs. Each point indicates a data point from each cell (a total of 10 cells for each condition). C3 transferase (C3), Y-27632 (Y27632), and blebbistatin (Blebb) decreased surface rigidity of rat MSCs and increased cell thickness. On the other hand, calyculin A (CalyA) and wiskostatin (Wisko) had little impact on these physical properties of MSCs. (C) Organization of pericellular actin cap of rat MSCs following treatment with the agents. The frequencies of organization of perinuclear actin cap are shown. The presence of the perinuclear actin cap at each condition was determined from more than 23 cells. The typical images for organization and disruption or not of the actin cap are shown in Supplementary Fig. S1. C3 transferase (C3), Y-27632 (Y27632), and blebbistatin (Blebb) decreased actin cap organization; calyculin A (CalyA) and wiskostatin (Wisko) increased actin cap organization. (D) Proliferation activity of rat MSCs cultured with various reagents. The cell number at 6 days was evaluated by measuring the cellular ATP contents with chemiluminescence system. C3 transferase (C3), Y-27632 (Y27632), and blebbistatin (Blebb) slightly increased the cell numbers; on the other hand, calyculin A (CalyA) and wiskostatin (Wisko) did not influence the proliferation.

log-normal distribution, and a median value of 9 points was adopted for the Young's modulus and the thickness of each cell.

2.4. Cell proliferation assay

Approximate cell numbers were determined using an ATP bioluminescence assay kit according to the manufacturer's instructions. Rat MSCs were plated at a density of 1×10^3 cells/well into white 96-well culture plates and cultured in the culture medium containing the cytoskeleton-modifying reagent for 6 days. The ATP bioluminescence reagent was added to the wells, and the cultured cells were shaken for 1 min and then incubated for another 10 min at 25 °C. Luminescence was measured with Synergy HT (BioTek, Winooski, VT).

2.5. Evaluation of perinuclear actin cap

The perinuclear actin cap was evaluated by staining the actin filaments of rat MSCs. Cells cultured for 2 days with the cytoskeleton-modifying reagent were fixed with 4% paraformaldehyde,

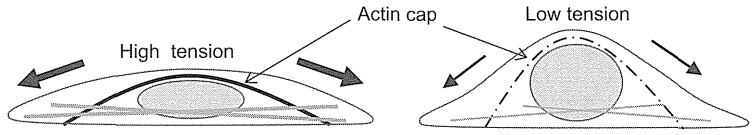

	Normal MSC	Stress fibers- attenuated MSC
Surface stiffness	Rigid	Elastic
Thickness	Low	High
Actin cap	Developed	Decreased
Tension source	Stress fibers	Isotropic cortex tension
Proliferation activity	Normal	Increased

Fig. 3. Overview of the physical properties of MSCs. In normal MSCs, developed perinuclear actin caps generate highly surface tension and press tightly against the nucleus, giving the cells a rigid surface stiffness and flat thickness. In contrast, in stress fibers-attenuated MSCs, the surface tension was decreased and the cell surface was boosted by the nucleus, resulting in the cells with elastic surfaces and a high thickness. Furthermore, elastic and tall cells tended to also have high proliferation activities.

permeabilized with 0.5% Triton X-100, and then stained with FITC-labeled phalloidin for actin filaments and propidium iodide for nucleus. Specimens were observed by confocal laser scanning microscopy (CLSM; FV-1000; Olympus, Tokyo, Japan) in 0.5 μm serial sections. The presence of the perinuclear actin cap was determined from the status of actin filaments over the nucleus in more than 23 cells for each condition (Supplementary Fig. S1).

3. Results

3.1. Relationship between stiffness and thickness of rat MSCs

First, we examined the relation between every AFM-measured Young's modulus and the thickness of each rat MSC (Supplementary Fig. S2). Compared with the thickness, the measured Young's modulus varied widely for each AFM manipulation (Supplementary Fig. S2). This was due to the fact that cellular mechanical properties are local and can change dramatically based on the location being probed [27]. Since it was difficult to determine the cell stiffness from these scattered Young's moduli, we examined the distribution of Young's moduli of rat MSCs in single cells and found that the distribution of Young's moduli corresponded to a log-normal pattern of distribution (Fig. 1B). Therefore, we selected the median value of the widely spread Young's moduli of each cell in this study, because the median provides a better estimate of the target value than the mean in a log-normal distribution.

Thickness versus Young's modulus of each adherent rat MSC was then plotted (Fig. 1C). Analyses of 100 cells revealed that Young's modulus of various adherent rat MSCs varied largely, and that it had a weak inverse correlation with cell thickness in each cell (Fig. 1C). The correlation coefficient R between these 2 factors was 0.35 ($P = 0.0004$). In short, flat, adherent MSCs tended to be rigid, whereas tall MSCs showed a relatively elastic property.

3.2. Regulation of cell stiffness and thickness of rat MSCs by actin cytoskeleton

An intact actin cytoskeleton contributes a major part of cell stiffness, yet there are several forms of actin cytoskeleton in a cell, e.g., stress fibers, lamellipodia, filopodia, and cortical actin. Here, we examined the effect of actin stress fibers and lamellipodia on stiffness and thickness of adherent rat MSCs, using several pharmacological agents that affect the actin cytoskeleton (Fig. 2A). We used gentle concentrations of all agents to avoid inducing obvious morphological changes (Supplementary Fig. S3).

Rho inhibitor C3 transferase, ROCK inhibitor Y-27632, and myosin II ATPase inhibitor blebbistatin prevent and attenuate stress fiber formation [28–30]. The Young's moduli of the cells treated with these agents decreased relatively while their thickness increased (Fig. 2B). On the other hand, the properties of the cells treated with myosin light chain phosphatase inhibitor calyculin A [31], which activates actomyosin formation and enhances actin polymerization in stress fibers, lamellipodia formation, and cortical actin, were hardly altered (Fig. 2B). Moreover, cells treated with the N-WASP inhibitor wiskostatin, which inhibits lamellipodia formation [32], showed no changes in either the Young's modulus or thickness (Fig. 2B). Thus, the cell stiffness and thickness of adherent rat MSCs were strongly affected by attenuated actin stress fibers, but were barely influenced by activation of actomyosin formation or inhibition of lamellipodia formation.

3.3. Perinuclear actin cap correlation with cell thickness and stiffness of rat MSCs

Actin filament structures that form a cap or dome located above the apical surface of the nucleus, referred to as the perinuclear actin cap, regulate the nuclear shapes of adherent fibroblasts [23]. The perinuclear actin cap is specifically disorganized or eliminated by the inhibition of actomyosin contractility. To identify a possible role of the perinuclear actin cap in regulation of stiffness and thickness of rat MSC, we examined the changes in the actin cap organization in rat MSC under the presence of each actin cytoskeleton-modifying agent by observing with CLSM.

The majority of rat MSCs had a well-developed perinuclear actin cap under normal culture conditions (Fig. 2C and Supplementary Fig. S1), rendering a flat shape to rat MSCs. Analysis of collected images demonstrated that treatment with actin stress fiber-formation inhibitors, namely, C3 transferase, blebbistatin, and particularly Y-27362, led to an increase in the number of cells with no actin cap as compared to the control cells (Fig. 2C and Supplementary Fig. S1). In contrast, more MSCs possessed an organized actin cap after treatment with calyculin A and wiskostatin (Fig. 2C). Attenuation of actin stress fibers results in reduction of perinuclear actin cap organization, which corresponds to the data of the cell thickness and stiffness of rat MSCs (Fig. 2B, C). On the other hand, augmentation of actin cap organization had little impact on the cell thickness and stiffness of rat MSCs (Fig. 2B, C).

3.4. Actin cytoskeleton affects proliferation activity of rat MSCs

Population thickness of adhered human MSCs may be related to proliferation activity at the donor level [3]. We thus examined the possible affect of actin cytoskeleton on proliferation activity of rat MSC population to determine whether cell stiffness relates with proliferation. Adding the agents to the cell culture media revealed that Y-27632, C3 transferase, and blebbistatin, which attenuate the actin stress fibers and the perinuclear actin cap, slightly increased the growth activity of rat MSCs (Fig. 2D). On the other hand, upregulation of perinuclear actin cap formation, as caused by treating the MSCs with wiskostatin or calyculin A, had little effect on cell

proliferation (Fig. 2D). These data consist with the results of cell thickness and stiffness. We therefore propose that actin cap organization regulates the proliferation activity and cell thickness and stiffness of rat MSC.

4. Discussion

In this study, we experimentally demonstrated two major points relevant to surface stiffness of substrate-adhering rat MSCs. One is that cell stiffness and cell thickness showed an inverse correlation at a single-cell level (Fig. 1C). The second is that the perinuclear actin cap organization regulates the cell stiffness, thickness, and possibly proliferation activity of rat MSCs (Fig. 2). A schematic diagram of our findings is shown in Fig. 3. Originally, MSCs adhere flat on a given substrate, and their actin stress fibers and perinuclear actin cap are well developed. A developed actin cap flattens out the nucleus and increases surface stiffness. On the other hand, cells with diminished stress fibers also lose their actin cap, with a resulting decrease in surface stiffness, and the nucleus boosts the cell height according to the plasticity of nuclear lamin A [23]. Thus, although surface stiffness and cell thickness are essentially different physical properties of cells, the perinuclear actin cap coordinates these properties in MSCs. However, these cell properties were not affected by augmentation of the actin cap organization after treatment with either calyculin A or wiskostatin (Fig. 2). In particular, calyculin A is an activator for actomyosin formation, and it increases surface stiffness in *Drosophila* embryonic S2R+ cells by accelerating cortical actin formation [21]. Cortical actin determines isotropic cortical tension of non-adherent or mitotic cell [33], and the surface stiffness of some cells is mainly determined by this cortical actin formation [21]. Thus, it is believed that anisotropic surface tension that arises from the perinuclear actin cap is higher than the isotropic cortical tension in MSCs, which would explain why behavior of the stiffness of rat MSCs differed from the above cell. In addition, further-developed stress fibers and actin cap of MSCs may induce partial buckling of the actin cytoskeleton [34] or fluidization of cell [35]; the physical properties are unaffected by augmentation of the actin cap formation. Interestingly, the stress fiber-attenuated MSCs tended to show a high proliferation activity (Fig. 2). This result corresponds with the previous study relating cell thickness with proliferation activity in human MSCs [3,4]. Our results additionally show that the states of the actin cap and actin stress fibers in MSCs are potent regulators of the proliferation activity of each cell.

It is well known that mechanical properties of cell environments control cell life [36,37]. In particular, commitment of differentiation lineage of MSCs is specified by matrix elasticity which is sensed by actomyosin contraction [38]. Furthermore, the surface stiffness of MSCs changes depending on the substrate elasticity. The surface stiffness of MSCs also changes during cell differentiation [39]. Our present study reveals that the surface stiffness of MSCs is regulated by actin stress fibers, including the perinuclear actin cap, and is related with proliferation activity. Thus, the mechanical properties of MSCs are potent indicators for their cell behavior and physiological functions. The evaluation of cell quality and estimation of cell activities of MSCs are essential cytotechnology for applications in regenerative medicine and tissue engineering. We predict that in the future non-destructive and high-speed methods of measuring mechanical properties of MSCs will become an essential part of the cytotechnology.

Acknowledgments

We thank Dr. Hajime Ohgushi (AIST) for kindly allowing us to use his facility. We thank Ms. Hiroko Machida (AIST) for generously helping with sample preparation. This work was supported by a grant from Okinawa Prefecture (Research Project of Industrialization of Medical Innovation and Technology).

Appendix A. Supplementary data

Supplementary data associated with this article can be found, in the online version, at doi:10.1016/j.bbrc.2011.04.022.

References

[1] F.P. Barry, J.M. Murphy, Mesenchymal stem cells: clinical applications and biological characterization, Int. J. Biochem. Cell. Biol. 36 (2004) 568–584.
[2] Z.J. Liu, Y. Zhuge, O.C. Velazquez, Trafficking and differentiation of mesenchymal stem cells, J. Cell. Biochem. 106 (2009) 984–991.
[3] Y. Katsube, M. Hirose, C. Nakamura, H. Ohgushi, Correlation between proliferative activity and cellular thickness of human mesenchymal stem cells, Biochem. Biophys. Res. Commun. 368 (2008) 256–260.
[4] A. Tokumitsu, S. Wakitani, M. Takagi, Noninvasive estimation of cell cycle phase and proliferation rate of human mesenchymal stem cells by phase-shifting laser microscopy, Cytotechnology 59 (2009) 161–167.
[5] J. Settleman, Tension precedes commitment-even for a stem cell, Mol. Cell 14 (2004) 148–150.
[6] R. McBeath, D.M. Pirone, C.M. Nelson, K. Bhadriraju, C.S. Chen, Cell shape, cytoskeletal tension, and RhoA regulate stem cell lineage commitment, Dev. Cell 6 (2004) 483–495.
[7] V.E. Meyers, M. Zayzafoon, J.T. Douglas, J.M. McDonald, RhoA and cytoskeletal disruption mediate reduced osteoblastogenesis and enhanced adipogenesis of human mesenchymal stem cells in modeled microgravity, J. Bone Miner. Res. 20 (2005) 1858–1866.
[8] S.E. Cross, Y.S. Jin, J. Rao, J.K. Gimzewski, Nanomechanical analysis of cells from cancer patients, Nat. Nanotechnol. 2 (2007) 780–783.
[9] J. Dai, M.P. Sheetz, Mechanical properties of neuronal growth cone membranes studied by tether formation with laser optical tweezers, Biophys. J. 68 (1995) 988–996.
[10] K.J. Van Vliet, G. Bao, S. Suresh, The biomechanics toolbox: experimental approaches for living cells and biomolecules, Acta Mater. 51 (2003) 5881–5905.
[11] H. Huang, R.D. Kamm, R.T. Lee, Cell mechanics and mechanotransduction: pathways, probes, and physiology, Am. J. Physiol. Cell Physiol. 287 (2004) C1–11.
[12] T. Kihara, C. Nakamura, M. Suzuki, S.W. Han, K. Fukazawa, K. Ishihara, J. Miyake, Development of a method to evaluate caspase-3 activity in a single cell using a nanoneedle and a fluorescent probe, Biosens. Bioelectron. 25 (2009) 22–27.
[13] T. Kihara, N. Yoshida, T. Kitagawa, C. Nakamura, N. Nakamura, J. Miyake, Development of a novel method to detect intrinsic mRNA in a living cell by using a molecular beacon-immobilized nanoneedle, Biosens. Bioelectron. 26 (2010) 1449–1454.
[14] K.D. Costa, Imaging and probing cell mechanical properties with the atomic force microscope, Methods Mol. Biol. 319 (2006) 331–361.
[15] A.M. Collinsworth, S. Zhang, W.E. Kraus, G.A. Truskey, Apparent elastic modulus and hysteresis of skeletal muscle cells throughout differentiation, Am. J. Physiol. Cell Physiol. 283 (2002) C1219–1227.
[16] W.R. Trickey, T.P. Vail, F. Guilak, The role of the cytoskeleton in the viscoelastic properties of human articular chondrocytes, J. Orthop. Res. 22 (2004) 131–139.
[17] I. Titushkin, M. Cho, Distinct membrane mechanical properties of human mesenchymal stem cells determined using laser optical tweezers, Biophys. J. 90 (2006) 2582–2591.
[18] H. Kagiwada, C. Nakamura, T. Kihara, H. Kamiishi, K. Kawano, N. Nakamura, J. Miyake, The mechanical properties of a cell, as determined by its actin cytoskeleton, are important for nanoneedle insertion into a living cell, Cytoskeleton (Hoboken) 67 (2010) 496–503.
[19] L. Lu, S.J. Oswald, H. Ngu, F.C. Yin, Mechanical properties of actin stress fibers in living cells, Biophys. J. 95 (2008) 6060–6071.
[20] A.S. Maddox, K. Burridge, RhoA is required for cortical retraction and rigidity during mitotic cell rounding, J. Cell Biol. 160 (2003) 255–265.
[21] P. Kunda, A.E. Pelling, T. Liu, B. Baum, Moesin controls cortical rigidity, cell rounding, and spindle morphogenesis during mitosis, Curr. Biol. 18 (2008) 91–101.
[22] T. Sugitate, T. Kihara, X.-Y. Liu, J. Miyake, Mechanical role of the nucleus in a cell in terms of elastic modulus, Curr. Appl. Phys. 9 (2009) e291–e293.
[23] S.B. Khatau, C.M. Hale, P.J. Stewart-Hutchinson, M.S. Patel, C.L. Stewart, P.C. Searson, D. Hodzic, D. Wirtz, A perinuclear actin cap regulates nuclear shape, Proc. Natl. Acad. Sci. USA 106 (2009) 19017–19022.
[24] T. Kihara, M. Hirose, A. Oshima, H. Ohgushi, Exogenous type I collagen facilitates osteogenic differentiation and acts as a substrate for mineralization of rat marrow mesenchymal stem cells in vitro, Biochem. Biophys. Res. Commun. 341 (2006) 1029–1035.
[25] H. Hertz, Über die berührung fester elastischer Körper, J. reine und angewandte Mathematik 92 (1881) 156–171.

[26] C. Rotsch, K. Jacobson, M. Radmacher, Dimensional and mechanical dynamics of active and stable edges in motile fibroblasts investigated by using atomic force microscopy, Proc. Natl. Acad. Sci. USA 96 (1999) 921–926.
[27] H. Huang, J. Sylvan, M. Jonas, R. Barresi, P.T. So, K.P. Campbell, R.T. Lee, Cell stiffness and receptors: evidence for cytoskeletal subnetworks, Am. J. Physiol. Cell Physiol. 288 (2005) C72–80.
[28] P. Chardin, P. Boquet, P. Madaule, M.R. Popoff, E.J. Rubin, D.M. Gill, The mammalian G protein rhoC is ADP-ribosylated by *Clostridium botulinum* exoenzyme C3 and affects actin microfilaments in Vero cells, EMBO J. 8 (1989) 1087–1092.
[29] M. Uehata, T. Ishizaki, H. Satoh, T. Ono, T. Kawahara, T. Morishita, H. Tamakawa, K. Yamagami, J. Inui, M. Maekawa, S. Narumiya, Calcium sensitization of smooth muscle mediated by a Rho-associated protein kinase in hypertension, Nature 389 (1997) 990–994.
[30] A.F. Straight, A. Cheung, J. Limouze, I. Chen, N.J. Westwood, J.R. Sellers, T.J. Mitchison, Dissecting temporal and spatial control of cytokinesis with a myosin II Inhibitor, Science 299 (2003) 1743–1747.
[31] H. Ishihara, H. Ozaki, K. Sato, M. Hori, H. Karaki, S. Watabe, Y. Kato, N. Fusetani, K. Hashimoto, D. Uemura, et al., Calcium-independent activation of contractile apparatus in smooth muscle by calyculin-A, J. Pharmacol. Exp. Ther. 250 (1989) 388–396.
[32] J.R. Peterson, L.C. Bickford, D. Morgan, A.S. Kim, O. Ouerfelli, M.W. Kirschner, M.K. Rosen, Chemical inhibition of N-WASP by stabilization of a native autoinhibited conformation, Nat. Struct. Mol. Biol. 11 (2004) 747–755.
[33] J. Fouchard, D. Mitrossilis, A. Asnacios, Acto-myosin based response to stiffness and rigidity sensing, Cell Adh. Migr. 5 (2011) 16–19.
[34] O. Chaudhuri, S.H. Parekh, D.A. Fletcher, Reversible stress softening of actin networks, Nature 445 (2007) 295–298.
[35] X. Trepat, L. Deng, S.S. An, D. Navajas, D.J. Tschumperlin, W.T. Gerthoffer, J.P. Butler, J.J. Fredberg, Universal physical responses to stretch in the living cell, Nature 447 (2007) 592–595.
[36] D.E. Discher, P. Janmey, Y.L. Wang, Tissue cells feel and respond to the stiffness of their substrate, Science 310 (2005) 1139–1143.
[37] D.E. Ingber, Cellular mechanotransduction: putting all the pieces together again, FASEB J. 20 (2006) 811–827.
[38] A.J. Engler, S. Sen, H.L. Sweeney, D.E. Discher, Matrix elasticity directs stem cell lineage specification, Cell 126 (2006) 677–689.
[39] E.M. Darling, M. Topel, S. Zauscher, T.P. Vail, F. Guilak, Viscoelastic properties of human mesenchymally-derived stem cells and primary osteoblasts, chondrocytes, and adipocytes, J. Biomech. 41 (2008) 454–464.

JOURNAL OF TISSUE ENGINEERING AND REGENERATIVE MEDICINE
J Tissue Eng Regen Med 2012;**6**: 261–271.
Published online 27 June 2011 in Wiley Online Library (wileyonlinelibrary.com) **DOI:** 10.1002/term.428

RESEARCH ARTICLE

A comparative study of induced pluripotent stem cells generated from frozen, stocked bone marrow- and adipose tissue-derived mesenchymal stem cells

Hiroe Ohnishi[1], Yasuaki Oda[1], Tetsuhiro Aoki[1,2], Mika Tadokoro[1], Yoshihiro Katsube[1]
Hajime Ohgushi[1], Koji Hattori[1] and Shunsuke Yuba[1]*

[1]*Tissue Engineering Research Group, Health Research Institute, National Institute of Advanced Industrial Science and Technology (AIST), Amagasaki site, Amagasaki, Hyogo, Japan*
[2]*Shinshu University, Department of Orthopaedic Surgery, Asahi, Matsumoto, Nagano, Japan*

Abstract

Bone marrow-derived mesenchymal stem cells (BMSCs) and adipose tissue-derived mesenchymal stem cells (AMSCs) have been used clinically for tissue regeneration; however, their proliferation/differentiation potentials are limited. Recently, induced pluripotent stem cells (iPSCs), known to have nearly unlimited potential to proliferate and differentiate into cells of all three germ layers, have gained wide interest in regenerative medicine. Here, we generated iPSCs from frozen-stocked AMSCs and BMSCs and examined their biological characteristics by comparative analyses. Although the iPSCs were more challenging to generate from the BMSCs than the AMSCs, both iPSC populations expressed pluripotent markers, such as stage-specific embryonic antigen (SSEA)-3, SSEA-4, tumour-related antigens (TRAs) TRA-1-60 and TRA-1-81, *OCT3/4* and *NANOG*. Furthermore, both cell populations differentiated well into three germ layer-derived cells, both *in vitro* and *in vivo*. These results indicate that iPSCs derived from frozen AMSCs/BMSCs exhibit equally acceptable iPSC characteristics and have potential in clinical applications as an alternative source of autogenous stem cells.

Received 2 July 2010; Accepted 13 March 2011

Keywords **induced pluripotent stem cells; mesenchymal stem cells; somatic stem cells; embryonic stem cells; adipose tissue; bone marrow; regenerative medicine; tissue engineering**

1. Introduction

Mesenchymal stem cells (MSCs) are somatic stem cells found in various tissues, such as bone marrow, adipose tissue, tooth germ, synovial membranes and umbilical cord blood (Kern *et al.*, 2006), and are known to differentiate into hepatocytes, neurocytes, cardiomyocytes, osteocytes, chondrocytes and adipocytes (Salem *et al.*, 2009). Due to their wide differentiation potential, they are currently used in regenerative medicine (Salem *et al.*, 2009). Since 2001, we have utilized BMSCs for bone or cartilage regeneration in orthopaedic patients (Morishita *et al.*, 2006; Ohgushi *et al.*, 1999, 2005). MSCs are also found in adipose tissue, which is readily obtained by liposuction (Fraser *et al.*, 2006; Hayashi *et al.*, 2008), and the AMSCs have recently been used for various regenerative medical treatments (Garcia-Olmo *et al.*, 2003, 2005; Gimble *et al.*, 2003, 2007; Lendeckel *et al.*, 2004; Yoshimura *et al.*, 2008). It has been reported that both BMSCs and AMSCs show similar cell surface antigen patterns, although the cells have some characteristic differences. In particular, BMSCs exhibit a more extensive bone-forming

*Correspondence to: Shunsuke Yuba, Tissue Engineering Research Group, Health Research Institute, National Institute of Advanced Industrial Science and Technology (AIST), 3-11-46 Nakoji, Amagasaki, Hyogo 661-0974, Japan.
E-mail: yuba-sns@aist.go.jp